20th AIAA Computational Fluid Dynamics Conference
27 - 30 June 2011, Honolulu, Hawaii

AIAA 2011-3854

High-Order CENO Finite-Volume Schemes for Multi-Block Unstructured Mesh

S. D. McDonald,* M. R. J. Charest,† and C. P. T. Groth‡
University of Toronto Institute for Aerospace Studies
4925 Dufferin Street, Toronto, Ontario, Canada, M3H 5T6

High-order discretization techniques remain an active area of research in Computational Fluid Dynamics (CFD) since they offer the potential to significantly reduce the computational costs necessary to obtain accurate predictions when compared to lower-order methods. In spite of the successes to date, efficient, universally-applicable, high-order discretizations remain somewhat illusive, especially for more arbitrary unstructured meshes. A novel, high-order, Central Essentially Non Oscillatory (CENO), cell-centered, finite-volume scheme is examined for the solution of the conservation equations of inviscid, compressible, gas dynamics on multi-block unstructured meshes. This scheme was implemented for both two- and three-dimensional meshes consisting of triangular and tetrahedral computational cells, respectively. The CENO scheme is based on a hybrid solution reconstruction procedure that combines an unlimited high-order k-exact, least-squares reconstruction technique with a monotonicity preserving limited piecewise linear least-squares reconstruction algorithm. Fixed central stencils are used for both the unlimited high-order k-exact reconstruction and the limited piecewise linear reconstruction. In the proposed hybrid procedure, switching between the two reconstruction algorithms is determined by a solution smoothness indicator that indicates whether or not the solution is resolved on the computational mesh. This hybrid approach avoids the complexities associated with reconstruction on multiple stencils that other essentially non-oscillatory (ENO) and weighted ENO schemes can encounter. As such, it is well suited for solution reconstruction on unstructured mesh. The CENO scheme for unstructured mesh is described and analyzed in terms of accuracy, computational cost, and parallel performance. In particular, the accuracy of reconstructed solutions for arbitrary functions and idealized flows is investigated as a function of mesh resolution. The ability of the scheme to accurately represent solutions with smooth extrema while maintaining robustness in regions of under-resolved and/or non-smooth solution content (i.e., solutions with shocks and discontinuities) is demonstrated for a range of problems.

I. Introduction

Computational fluid dynamics (CFD) has proven to be an important enabling technology in many areas of science and engineering. In spite of the relative maturity and widespread success of CFD in aerospace engineering, there is a variety of physically-complex flows which are still not well understood and are very challenging to predict by numerical methods. Such flows include but are not limited to: (i) multiphase, turbulent, and combusting flows encountered in propulsion systems (e.g., gas turbine engines and solid propellant rocket motors); (ii) compressible flows of conducting fluids and plasmas; and (iii) micro-scale non-equilibrium flows, such as those encountered in micro-electromechanical systems. These flows present numerical challenges as they generally involve a wide range of complicated physical/chemical phenomena and scales.

High-order methods have the potential to significantly reduce the cost of modelling physically-complex flows, but this potential is challenging to fully realize. As such, the development of robust and accurate high-order methods remains an active area of research. Standard lower-order methods (i.e, methods up to second

*M.A.Sc Candidate, UTIAS, smcdonald@utias.utoronto.ca.
†Post-Doctoral Fellow, UTIAS, charest@utias.utoronto.ca, Student Member AIAA.
‡Professor, UTIAS, groth@utias.utoronto.ca, Senior Member AIAA.

order) can exhibit excessive numerical dissipation for multi-dimensional problems and are often not practical for physically-complex flows. High-order methods offer improved numerical efficiency when accurate solution representations are sought since fewer computational cells are required to achieve a desired level of accuracy.[1] For hyperbolic conservation laws and/or compressible flow simulations, the main challenge involves obtaining accurate discretizations while ensuring that discontinuities and shocks are handled reliably and robustly.[2] High-order schemes for elliptic partial differential equations (PDEs) that govern diffusion processes should satisfy a maximum principle, even on stretched/distorted meshes, while remaining accurate.[3] There are many studies of high-order schemes developed for finite-volume,[2,4–12] discontinuous Galerkin,[13–17] and spectral finite-difference/finite-volume methods[18–22] on both structured and unstructured mesh. In spite of the these advances, there is still no consensus for a robust, efficient, and accurate scheme that fully deals with all of the aforementioned issues and is universally applicable to arbitrary meshes.

Harten *et al.*[2] originally proposed the essentially non-oscillatory (ENO) high-order finite-volume scheme which achieves monotonicity by avoiding the use of computational stencils that contain discontinuities. Weighted ENO (WENO) schemes attempt to simplify the ENO procedure by adopting a stencil-weighting approach.[8,10,11] However, both the ENO and WENO schemes encounter difficulties when selecting appropriate stencils on general multi-dimensional unstructured meshes[5,6,9,23] and using these stencils can produce poor conditioning of the linear systems involved in performing the solution reconstruction.[9,23] These difficulties, along with the associated computational cost and complexities of the ENO and WENO finite-volume schemes, limit the applicable range of ENO and WENO. Recently, Ivan and Groth[24,25] proposed a high-order central ENO (CENO) finite-volume scheme which attempts to address the limitations of ENO discretizations. A variant of the ENO scheme, the CENO scheme avoids the previously discussed complexities through the use of a fixed central stencil. A central stencil in general provides the most accurate reconstruction because of the cancellation of truncation errors. The hybrid scheme first performs the unlimited, high-order, k-exact least-squares reconstruction described by Barth.[4] If under-resolved solution content or discontinuities/shocks are detected, the scheme locally reverts to a monotonicity preserving limited, piecewise, linear, least-squares reconstruction procedure. Automatic switching is controlled by a solution smoothness indicator. As a result, CENO reconstruction effectively eliminates the appearance of $O(1)$ numerical oscillations in under-resolved regions and in solutions that contain strong discontinuities and/or shocks. Although uniform accuracy is not achieved for non-smooth solutions, the method is readily extendable to both multi-dimensions and unstructured mesh. The ability to formulate high-order schemes for unstructured computational meshes in a straightforward manner is particularly appealing for applications involving practical, complex, three-dimensional geometries.

This study considers the further development of the promising CENO finite-volume schemes of Ivan and Groth[24,25] to unstructured mesh. In particular, cell-centered CENO schemes are examined for the solution of the conservation equations of inviscid, compressible, gas dynamics on multi-block, unstructured meshes in both two- and three-dimensions using triangular and tetrahedral computational cells, respectively. As noted above, the hybrid approach avoids the complexities associated with other ENO and WENO schemes and does not require reconstruction on multiple stencils which, in some cases, can produce poorly conditioned coefficient matrices. CENO is therefore well suited for solution reconstruction on unstructured mesh. Following a description of the proposed scheme, the CENO scheme is analyzed in terms of accuracy, computational cost, and parallel performance. In particular, the accuracy of reconstructed solutions for arbitrary functions on unstructured mesh is examined and the influence of mesh resolution on accuracy is assessed for several idealized two- and three-dimensional flow problems. The ability of the scheme to accurately represent solutions with smooth extrema yet robustly handle under-resolved and/or non-smooth solution content (i.e., solutions with shocks and discontinuities) is demonstrated for a range of problems.

II. CENO Finite-Volume Scheme

A. Hyperbolic Conservation Equations

The conservation equations of interest herein are the Euler equations governing inviscid, compressible, gaseous flow. In three space dimensions, these are non-linear partial-differential equations take the form

$$\frac{\partial \mathbf{U}}{\partial t} + \frac{\partial \mathbf{F}}{\partial x} + \frac{\partial \mathbf{G}}{\partial y} + \frac{\partial \mathbf{H}}{\partial z} = 0 \tag{1}$$

where the conserved solution vector, $\mathbf{U}$, and fluxes in the x-, y- and z-direction, $\mathbf{F}$ and $\mathbf{G}$, respectively, are defined as

$$\mathbf{U} = \begin{bmatrix} \rho \\ \rho u \\ \rho v \\ \rho w \\ e \end{bmatrix}, \quad \mathbf{F} = \begin{bmatrix} \rho u \\ \rho u^2 + p \\ \rho uv \\ \rho uw \\ u(e+p) \end{bmatrix}, \quad \mathbf{G} = \begin{bmatrix} \rho v \\ \rho uv \\ \rho v^2 + p \\ \rho vw \\ v(e+p) \end{bmatrix}, \quad \text{and} \quad \mathbf{H} = \begin{bmatrix} \rho w \\ \rho uw \\ \rho vw \\ \rho w^2 + p \\ v(e+p) \end{bmatrix} \tag{2}$$

Here ρ is the density, u, v, and w are the components of the fluid velocities in the x-, y-, and z-directions, e is the total energy, and p is the pressure. The total energy is defined as

$$e = \frac{p}{\gamma - 1} + \frac{\rho}{2}(u^2 + v^2 + w^2) \tag{3}$$

and density is related to pressure by

$$p = \frac{\rho a^2}{\gamma} \tag{4}$$

where γ is the specific heat ratio for the gas of interest (taken to be $7/5 = 1.4$ for all the problems considered herein) and a is the sound speed.

B. Finite-Volume Scheme

In the proposed cell-centered finite-volume approach, the physical domain is discretized into finite-sized computational cells and the integral forms of conservation laws are applied to each individual cell. For a cell i, the approach results in the following coupled system of partial differential equations (PDEs) for cell-averaged solution quantities:

$$\frac{\mathrm{d}\overline{\mathbf{U}}_i}{\mathrm{d}t} = -\frac{1}{V_i} \oiint_S \overrightarrow{\mathbf{F}} \cdot \hat{n} \, \mathrm{d}\mathcal{A} \tag{5}$$

where V_i is the cell volume, $\overrightarrow{\mathbf{F}}$ is the flux dyad, $\mathcal{A}$ is the area of the face and $\hat{n}$ is the unit vector normal to a given edge. Applying Gauss quadrature to evaluate the surface integral produces a set of nonlinear ordinary differential equations (ODEs) given by

$$\frac{\mathrm{d}\overline{\mathbf{U}}_i}{\mathrm{d}t} = -\frac{1}{V_i} \sum_{l=1}^{N_\mathrm{f}} \sum_{m=1}^{N_\mathrm{G}} \left(\omega \overrightarrow{\mathbf{F}} \cdot \hat{n} \mathcal{A} \right)_{i,l,m}, \tag{6}$$

where N_f is the number of faces (equal to 3 for two-dimensional triangles and 4 for three-dimensional tetrahedra), N_G is the number of Gauss quadrature points and ω is the quadrature weight. The number of Gauss quadrature points required along each face is a function of the reconstruction order and number of spatial dimensions. For two-dimensional meshes of triangles, one quadrature point is used for linear (k=1) reconstruction while two quadrature points are used for quadratic (k=2) and cubic (k=3) reconstruction. Similarly, one, three, and four quadrature points are used for k=1, 2, and 3 reconstruction on three-dimensional meshes of tetrahedral cells.

The numerical flux at the quadrature points along the cell interfaces is computed by interpolating the solution in each adjacent cell and solving a Riemann problem in a direction aligned along the face normal. Roe's approximate Riemann solver[26,27] was used throughout this work along with the correction proposed by Harten *et al.*[28] to ensure that the entropy condition is never violated at the sonic point. The left and right solution states at the interface are determined using a k-order CENO reconstruction scheme.[24,29–31]

C. CENO Reconstruction

The high-order CENO method uses a hybrid solution reconstruction process rather than adapting or weighting multiple stencils.[24,25] This hybrid approach involves a fixed central stencil in smooth or fully-resolved regions which is switched to a limited piecewise linear reconstruction when discontinuities in solution content are encountered. This switching provides a means of eliminating spurious oscillations that can occur near regions where the solution is under-resolved. It is facilitated by a parameter called the smoothness indicator which indicates the current level of resolution.

1. k-Exact Reconstruction

The CENO spatial discretization scheme is based on the high-order k-exact least-squares reconstruction technique of Barth.[4] The k-exact higher-order reconstruction algorithm begins by assuming that the solution within each cell can be represented by the following Taylor series expansion in three dimensions:

$$u_i^k(x,y,z) = \sum_{p_1=0}^{k} \sum_{p_2=0}^{k} \sum_{p_3=0}^{k} (x-x_i)^{p_1} (y-y_i)^{p_2} (z-z_i)^{p_3} D_{p_1 p_2 p_3} \tag{7}$$

where u_i^k is the reconstructed primitive or conserved solution quantity, (x_i,y_i,z_i) are the coordinates of the cell centroid, k is the order of the piecewise polynomial interpolant and $D_{p_1 p_2 p_3}$ are the unknown coefficients of the Taylor series expansion. The summation indices, p_1, p_2 and p_3, must always satisfy the condition that $(p_1 + p_2 + p_3) \leq k$.

The following conditions are applied to determine the unknown coefficients: i) the solution reconstruction must reproduce polynomials of degree $N \leq k$ exactly; ii) the mean or average value within the computational cell must be preserved; and iii) the reconstruction must have compact support. The second condition states that

$$\bar{u}_i = \frac{1}{V_i} \iiint_{V_i} u_i^k(x,y,z)\, \mathrm{d}V \tag{8}$$

where $\bar{u}_i$ is the cell average. The third condition dictates the number and location of neighboring cells included in the reconstruction. For a compact stencil, the minimum number of neighbors is equal to the number of unknowns minus one (because of the constraint imposed by Eq. (8)). For any type of mesh, the total number of unknown coefficients for a particular order is given by

$$N = \frac{1}{d!} \prod_{n=1}^{d} (k+n)\,, \tag{9}$$

where d represents the number of space dimensions. In two-dimensions, there are six unknown coefficients for k=2 and ten for k=3. In three-dimensions, there are ten and twenty unknown coefficients for k=2 and k=3, respectively.

Additional neighbors are included to ensure that the stencil is not biased in any particular direction and that the reconstruction remains reliable on poor quality meshes with high aspect ratio cells.[24] For each neighboring cell, p, a constraint is formed by requiring that

$$\bar{u}_p = \frac{1}{V_p} \iiint_{V_p} u_i^k(x,y,z)\, \mathrm{d}V \tag{10}$$

Since the above constraints result in an over-determined system of linear equations, a least-squares solution for the coefficients, $D_{p_1 p_2 p_3}$, is obtained in each cell. Note that the coefficient matrix of the linear system depends only on the mesh geometry and can be partially calculated and stored prior to computations. Either a Householder QR factorization algorithm or orthogonal decomposition by the SVD method was used to solve the weighted least squares problem.[32] Weighting was applied to each control volume to improve the locality of the reconstruction.[33] Typically, an inverse distance weighting formula was applied,

$$w_j = \frac{1}{|\vec{x}_j - \vec{x}_i|}, \tag{11}$$

where $\vec{x}_j$ is the centroid of the neighbor cell j.

2. Smoothness Indicator

After performing a k-exact reconstruction for each solution variable in each computational cell, the smoothness indicator is computed for every reconstructed variable. It is evaluated as

$$S = \frac{\alpha}{\max((1-\alpha), \epsilon)} \frac{(SOS - DOF)}{DOF - 1} \tag{12}$$

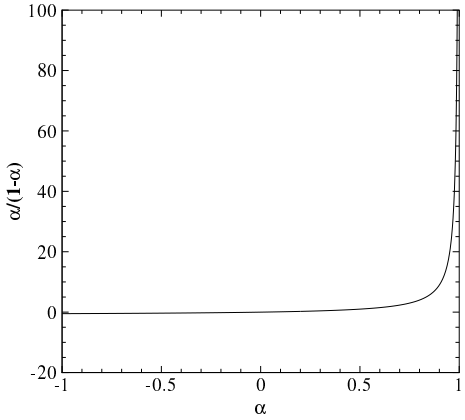

Figure 1. Variation of smoothness indicator with α.

where α is a smoothness parameter, ϵ is a tolerance to avoid division by zero (equal to 10^{-8} here), DOF is the number of degrees off freedom and SOS is the size of the stencil. The smoothness parameter, α, for a cell i is given by

$$\alpha = 1 - \frac{\sum_p (u_p^k(x_p, y_p, z_p) - u_i^k(x_p, y_p, z_p))^2}{\sum_p (u_p^k(x_p, y_p, z_p) - \overline{u}_i)^2} \tag{13}$$

where u is the solution variable of interest, the subscript p refers to the cells in the reconstruction stencil, $u_p^k(x_p, y_p, z_p)$ is the reconstructed solution in cell p evaluated at the cell's centroid (x_p, y_p, z_p), $u_i^k(x_p, y_p, z_p)$ is the projected value of the reconstruction polynomial for cell i evaluated at (x_p, y_p, z_p), and $\overline{u}_i$ is the average value for cell i. By definition, α can have a value between negative infinity and one. A value of unity indicates that the solution is smooth whereas small or negative values indicate large variations in solution content within the reconstruction stencil.

The behavior of the smoothness indicator is demonstrated in Fig. 1. As α approaches unity, the smoothness indicator grows rapidly. Solutions are deemed smooth when the value of S is above critical value, S_c. Previous studies found that values for S_c between 1000–5000 provided an excellent balance between stability and accuracy.[24,29] Typical values for S in smooth regions tend to be orders of magnitude greater than these cutoff limits. Unless otherwise specified, a value for S_c of 1000 was used.

The proposed CENO scheme attempts to preserve monotonicity by reverting the high-order k-exact reconstruction to a limited piecewise linear (k=1) reconstruction when S is below the critical value. The slope limiter developed by Venkatakrishnan[34] was employed here.

D. Time-Marching Schemes

For all of the transient cases considered in this work, a multi-stage explicit time-marching scheme was used to solve the ODEs given by Eq. (6). Either a two-stage or four-stage standard Runge-Kutta scheme is used depending on the desired spatial accuracy.

III. Unstructured Mesh

Two-dimensional and three-dimensional unstructured meshes of triangular and tetrahedral cells, respectively, were generated using Gmsh, a finite element mesh generator.[35] A flexible block-based data-structure is adopted here to since one of the goals of this research is to develop a highly-scalable solution algorithm applicable for large-scale distributed-memory computer architectures. As such, the mesh was divided into blocks via domain decomposition using PMETIS.[36] This block-based approach facilitates dynamic load balancing when used in combination with adaptive mesh refinement (AMR).[37–39]

Representation of unstructured meshes requires a connectivity table to explicitly define the connections

between points.[40] Typical data structures can range from finite element data structures, edge structures, vertex lists, and quad-edge structures.[41] The data structure implemented here is an edge-type structure which lists the connectivity of vertices and adjacent faces by storing a quadruple of each edge. This quadruple consists of the origin and destination of each edge as well as two faces/cells which share that edge. This type of data structure allows one to easily traverse through the mesh.[41] It is especially advantageous for flux-based finite-volume schemes. A similar procedure was employed for three-dimensional meshes.

For simplicity, staggered or dual meshes were not employed in either two- or three-dimensions. Instead, the computational cells were defined by the vertices and only the average solution for each computational cell was stored and used to compute the polynomial coefficients. By avoiding the use of staggered grids and utilizing a block-based grid structure, the proposed high-order unstructured finite-volume scheme is well suited for use in combination with AMR.[37,42–44]

IV. Results For Two-Dimensional Unstructured Mesh

Numerical results obtained using the proposed cell-centered CENO finite-volume scheme for several two-dimensional function reconstructions and unsteady test flow problems are now described in this section. The two-dimensional results have been obtained for multi-block unstructured mesh consisting of triangular computational cells.

A. Spherical Cosine Function

The first case considered is the reconstruction of a smooth spherical cosine function. The function, which is smooth in both the x- and y-directions, is described by

$$u(r) = 1 + \frac{1}{3}\cos(r) \tag{14}$$

where $r = \sqrt{x^2 + y^2}$ is the radial position. The solution is computed on a domain of size 20×20 and centered on $x = y = 0$ using various grid resolutions.

The results for this reconstruction performed on a mesh with 92,040 triangular elements and 46,419 nodes are shown in Fig. 2. The $k = 3$ reconstruction accurately captures the smooth variation in the solution. The effect of grid resolution on the L_1 norm of the error in the numerical solution is illustrated in Fig. 3 for various values of k. As expected, the k-exact reconstruction yields the correct order of accuracy for smooth functions.

B. Abgrall's Function

The Abgrall function[5] possesses a number of solution discontinuities which test a high-order spatial discretization's ability to maintain monotonicity. Reconstructions of this function using the proposed high-order CENO algorithm for unstructured meshes are obtained here to ensure the effectiveness of the smoothness indicator defined in Eq. (2). Even though the performance of this formulation for S was already verified using the Abgrall function and structured mesh,[24,29] it has not been evaluated for unstructured mesh. The Abgrall function is defined as

$$u(x,y) = \begin{cases} f(x - \cot\sqrt{\frac{\pi}{2}}\, y) & \text{if } x \le \frac{\cos\,\pi y}{2}, \text{ and} \\ f(x + \cot\sqrt{\frac{\pi}{2}}\, y) + \cos(2\pi y) & \text{if } x > \frac{\cos\,\pi y}{2}. \end{cases} \tag{15}$$

where

$$f(r) = \begin{cases} -r\sin\left(\frac{3\pi}{2}r^2\right) & \text{if } r \le -\frac{1}{3}, \\ |\sin(2\pi r)| & \text{if } |r| < \frac{1}{3}, \text{ and} \\ 2r - 1 + \frac{1}{6}\sin(3\pi r) & \text{if } r \ge \frac{1}{3}. \end{cases} \tag{16}$$

and $r = \sqrt{x^2 + y^2}$.

The reconstructed solution (k=3) obtained for a mesh with 91,890 elements and 46,344 nodes is depicted in Fig. 4. A value for the smoothness indicator cutoff equal to 2500 was employed for this test case. As

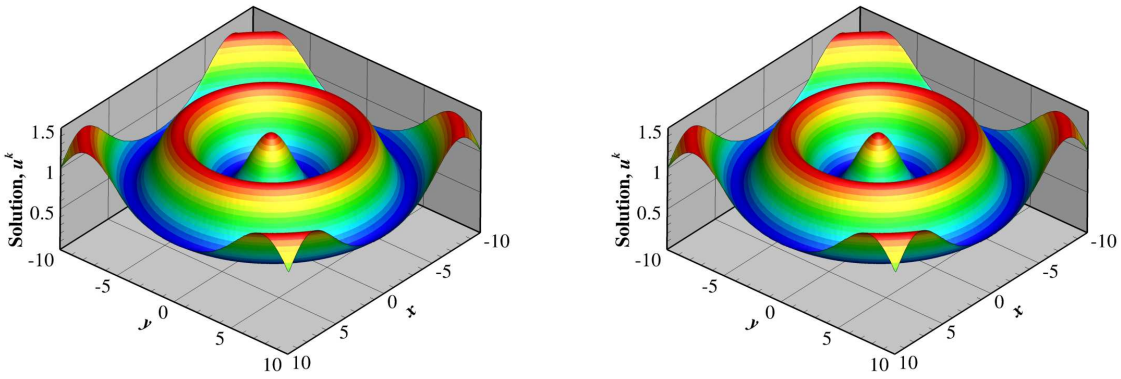

(a) Exact solution (b) Reconstructed solution ($k = 3$)

Figure 2. Reconstructed solution for the spherical cosine function obtained on a mesh with 92,040 triangular elements and 46,419 nodes.

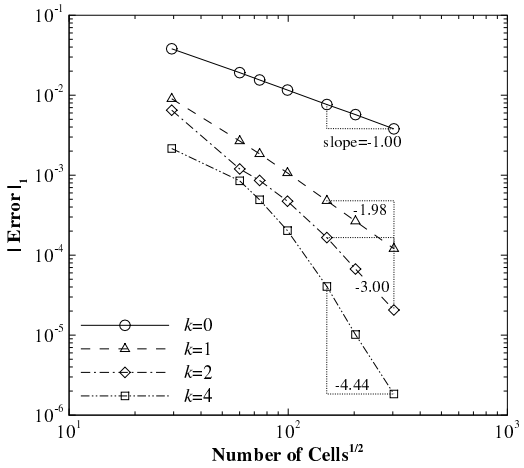

Figure 3. Effect of grid resolution on solution accuracy for the spherical cosine function. Accuracy is measured using the L_1 norm of the error.

observed in the figure, the CENO scheme was able to accurately reconstruct the Abgrall function without producing spurious oscillations.

The effect of mesh resolution on the L_1 norm of the solution error is shown in Fig. 5(a). Only a slight improvement in the order of accuracy is achieved by increasing k from 0 to 3, but the error in the reconstructed solution is substantially lower for k=3. The k=0 reconstruction required 91,890 elements to produce an error less than 0.045, while the k=3 reconstruction can obtain a similar level of accuracy with only 9916 elements.

The first-order behavior displayed by the k=3 reconstruction is attributed to the existence of discontinuities in Eq. (15). This is verified by the contour plot of the smoothness indicator obtained for k=3 which is illustrated in Fig. 5(b). The smoothness indicator correctly identified the discontinuities in Abgrall's function and the CENO algorithm locally reverted to the piecewise linear limited reconstruction procedure described in Section 2. As a result, spurious non-physical oscillations were avoided and monotonicity was maintained.

C. Shock-Box Problem

As a first step to demonstrating the robustness of the proposed high-order finite-volume scheme for multi-block unstructured meshes, transient solutions for a two-dimensional shock-box were obtained. This ideal test cases involves a square enclosure which initially contains high- and low-pressure air separated by a diaphragm. At time t=0, the diaphragm is burst and complex wave structures travel through the domain.

The prescribed initial conditions are

$$\rho = 1.225 \text{ kg/m}^3, \quad u = v = 0 \text{ m/s}, \quad p = 101.325 \text{ kPa} \tag{17}$$

for $x \geq 0$ and $y \geq 0$ and

$$\rho = 4.9 \text{ kg/m}^3, \quad u = v_r = 0 \text{ m/s}, \quad p = 1,013.25 \text{ kPa} \tag{18}$$

for $x < 0$ and $y < 0$.

The density of the gas in the shock-box at t=7 ms computed using CENO with zeroth- and third-order polynomial interpolants is shown in Fig. 6. Both of these results were obtained using a mesh consisting of 28,482 triangular elements with 14,464 nodes. Both solutions display a distinct symmetry about an axis passing through (x, y)=$(-5 \text{ m}, -5 \text{ m})$ and $(5 \text{ m}, 5 \text{ m})$. The figure clearly shows a significant improvement in resolution when higher-order polynomial interpolants are used.

The smoothness indicator for density computed at t=7 ms is illustrated at Fig. 7. Areas which are shown in red have been flagged as non-smooth. As expected, these flagged regions correspond to locations in which a discontinuity exists.

D. Cylindrical Expansion

A two-dimensional cylindrically-symmetric homentropic expansion was also studied here. This test case consists of a square enclosure which initially contains air with a radial pressure distribution. The initial distribution for radial velocity, u_r, is given by

$$u_r = \begin{cases} 0 & \text{if } r \leq \frac{1}{2}, \\ \frac{1}{\gamma}(1 + \tanh \frac{r-1}{0.25-(r-1)^2}) & \text{if } \frac{1}{2} < r < \frac{3}{2}, \text{ and} \\ \frac{2}{\gamma} & \text{if } r \geq \frac{3}{2} \end{cases} \tag{19}$$

where the other flow quantities are obtained from the following relations:

$$u_r + \frac{2}{\gamma - 1} a = \frac{2}{\gamma - 1}, \quad \rho = \gamma a^{\frac{2}{\gamma - 1}}, \quad p = \frac{\rho a^2}{\gamma} \tag{20}$$

with $r = \sqrt{x^2 + y^2}$ and $\theta = \arctan \frac{y}{x}$.

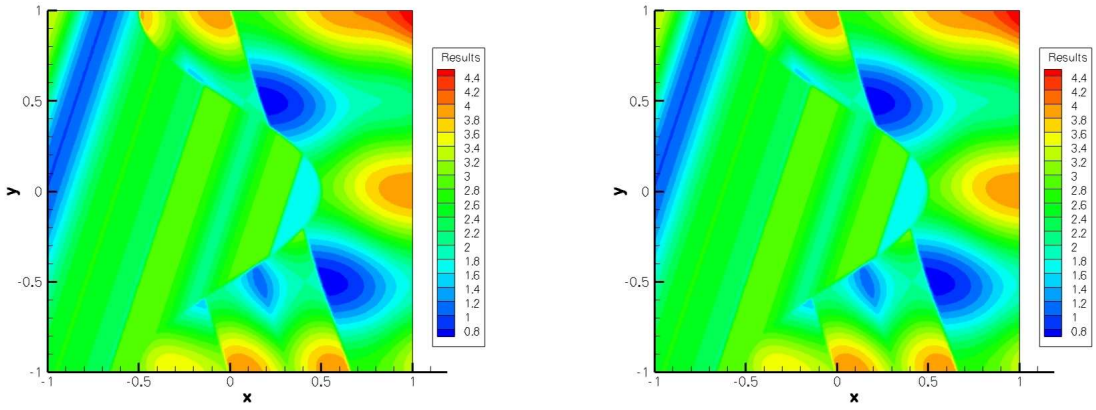

(a) Exact solution

(b) Reconstructed solution ($k = 3$)

Figure 4. Reconstructed solution of Abgrall's function on a mesh with 91,890 triangular elements and 46,344 nodes.

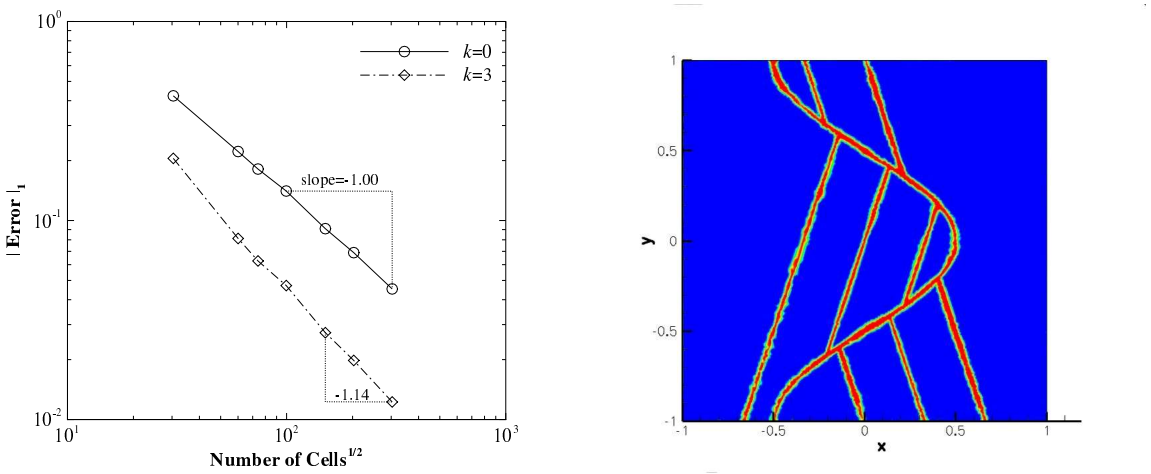

(a) (b)

Figure 5. (a) Effect of grid resolution on the L_1 norm of the solution error and (b) the computed smoothness indicator for the k=3 reconstruction of Abgrall's function.

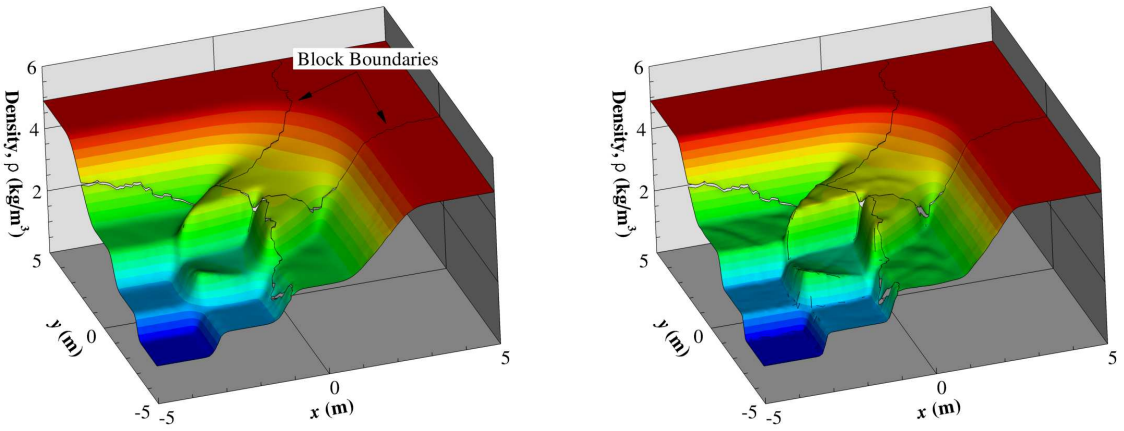

(a) k=0 (b) k=3

Figure 6. Computed density for the two-dimensional shock-box at t=7 ms obtained using CENO. Block boundaries are projected onto the contours.

The density inside the domain computed using a fourth-order reconstruction (k=3) after 0.5 ms have elapsed are shown in Fig. 8. It was computed using a computational mesh with 12,546 triangular elements and 6,422 nodes.

The effect of mesh resolution on the solution accuracy is studied for various polynomial interpolants. Here, accuracy was measured by the L_1 norm of the solution error. The results are illustrated in Fig. 9. As expected, both the first- (k=0) and third-order (k=2) solutions achieve the correct slope. The fourth-order reconstruction does not quite achieve a theoretical slope of 4, which indicates that asymptotic convergence has not yet been achieved on the finest mesh considered here.

V. Results For Three-Dimensional Unstructured Mesh

The finite-volume procedure is currently being extended to incorporate three-dimensional multi-block unstructured mesh of tetrahedrons. A sample multi-block grid is illustrated in Fig. 10. Numerical results

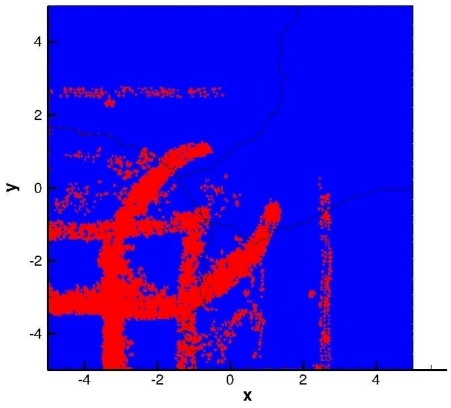

Figure 7. The smoothness indicator for the density variable at t=7 ms computed for a k=3 reconstruction. Areas which are shown in red have been flagged as non-smooth.

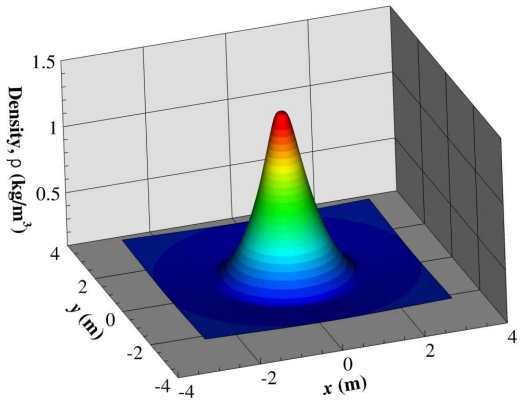

Figure 8. Effect of mesh resolution on the L_1 norm of the solution error for the cylindrical expansion.

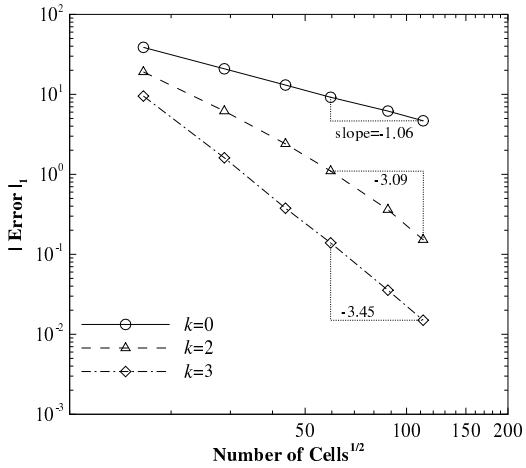

Figure 9. Computed density contours for two-dimensional cylindrical at t=0.5 ms. The solution was obtained on a a computational mesh with 12,546 triangular elements and 6,422 nodes.

for both smooth and discontinuous three-dimensional function reconstructions are described below.

A. Spherical Cosine Function

The first case considered in three dimensions is the reconstruction of the smooth spherical cosine function examined in Sec. IV. The function is described by Eq. (14) except with $r = \sqrt{100x^2 + 100y^2 + 100z^2}$. The solution is computed on a domain of size $1 \times 1 \times 1$ and centered on $x = y = z = 0.5$ using various grid resolutions. The exact solution is illustrated in Fig. 11(a).

The results for the unlimited k-exact reconstruction of the three-dimensional spherical cosine function performed on a mesh with 4,071 tetrahedral elements is illustrated in Fig. 11(b). As the order of the piecewise polynomial interpolant is increased from k=0 to k=4, the reconstructed solution rapidly approaches the exact solution. An analysis of the L_1 norm of the error in the numerical solution as the mesh resolution is increased, illustrated in Fig. 11(c) for various values of k, confirms that k-exact reconstruction of a smooth function yields an order of accuracy equal to k+1.

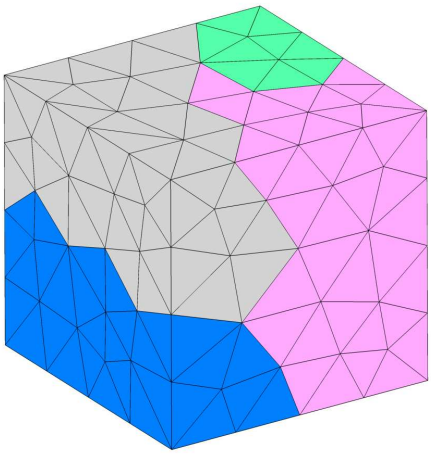

Figure 10. A sample three-dimensional multi-block unstructured mesh of tetrahedrons. The different colors designate different mesh blocks.

B. Abgrall's Function

The Abgrall function[5] was applied in three dimensions by extruding the two-dimensional function (Eq. (15)) along the z axis. The reconstructed solution obtained using the proposed high-order CENO algorithm for unstructured meshes with $k = 4$ is illustrated in Fig. 12. As observed in Fig. 12(b), the CENO scheme was able to accurately reconstruct the Abgrall function without producing spurious oscillations on a relatively coarse mesh of 232,335 computational cells. The smoothness indicator, illustrated in Fig. 12(a), correctly identified the discontinuities in both $f(r)$ and $\frac{\partial f(r)}{\partial x}$.

The reconstructed solution obtained with k=0 to k=4 along a line is illustrated in Fig. 13(a). The proposed CENO scheme is able to ensure oscillation-free solutions despite the large discontinuities observed. Note that the spikes observed in the reconstructed solutions are an undesired artifact of post-processing. The automatic switching procedure is demonstrated in Fig. 13(b) for k=3.

The effect of mesh resolution on the L_1 norm of the solution error is shown in Fig. 14. Only a slight improvement in the order of accuracy is achieved by increasing k from 0 to 2, but there error in the reconstructed solution is substantially lower for k=2 and higher.

VI. Conclusion

A high-order finite-volume solver has been implemented for the numerical solution of the compressible Euler equations on multi-block unstructured meshes. The scheme is a high-order variant of cell-centered, Godunov-type, finite-volume, methods and uses the hybrid CENO reconstruction method recently proposed by Ivan and Groth.[24,29–31]

Results in two and three dimensions has provided an initial validation of the CENO reconstruction procedure and finite-volume scheme. This initial validation has considered the high-order reconstruction of functions. Third- and forth-order accuracy was achieved on general unstructured triangular and tetrahedral mesh. Additionally, the smoothness indicator was proven to work as anticipated, lowering the order of accuracy of the scheme near areas of discontinuities in order to maintain monotonicity.

Further validation was shown for predicted solutions to the two-dimensional Euler Equations. Two unsteady flow problems were investigated: a shock-box problem and a cylindrical expansion. The shock box case showed more accurate results for the high-order scheme as compared to the standard low-order method and the smoothness indicator performed as expected. The cylindrical expansion problem illustrated that high-order solutions can be achieved on unstructured mesh when computing the solution to smooth inviscid compressible fluids. In general, the ability of the prosed scheme to accurately represent solutions with smooth extrema and yet robustly handle under-resolved and/or non-smooth solution content has been

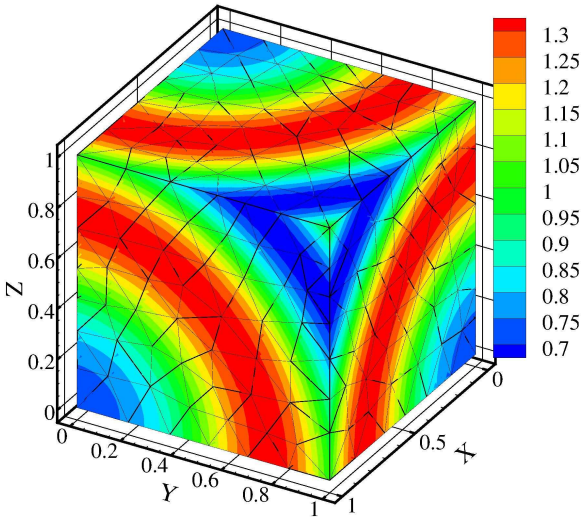

(a) Exact Solution

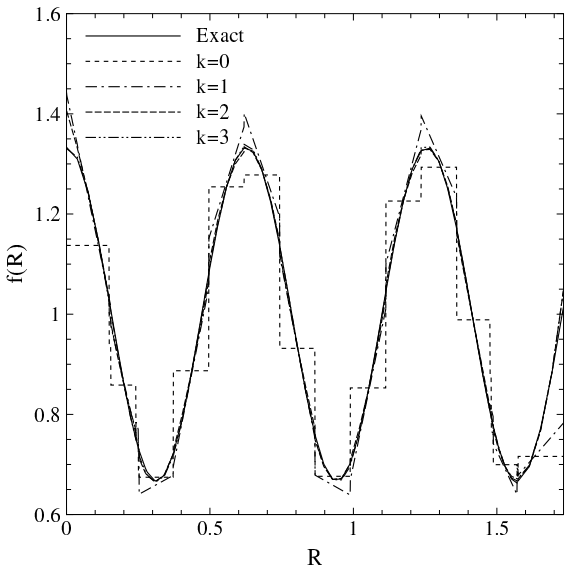

(b) Reconstructed solution along the diagonal from $x = y = z = 0$ to $x = y = z = 1$. The solution was obtained on a mesh with 4,071 tetrahedral elements.

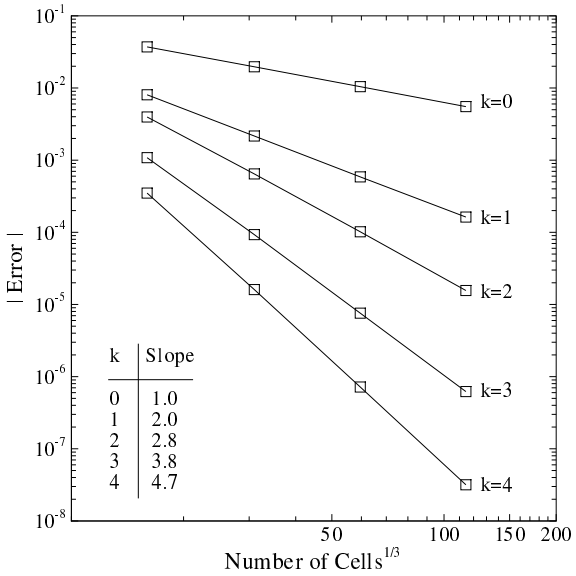

(c) Effect of grid resolution on solution accuracy. Accuracy is measured using the L_1 norm of the error.

Figure 11. Results for k-exact reconstruction of the spherical cosine function in three-dimensions.

demonstrated.

Future work includes further development and validation of the proposed CENO algorithm for both two- and three-dimensional unstructured meshes of triangular and tetrahedral cells. The proposed algorithm will also be combined with a multi-block AMR algorithm.[37, 42–44] The applicability of CENO to AMR and the substantial benefits in terms of accuracy and computational savings have already been demonstrated for body-fitted multi-block meshes.[24, 29–31]

References

[1]Pirozzoli, S., "On the spectral properties of shock-capturing schemes," *Journal of Computational Physics*, Vol. 219, No. 2, 2006, pp. 489–497.

[2]Harten, A., Enquist, B., Osher, S., and Chakravarthy, S. R., "Uniformly High Order Accurate Essentially Non-Oscillatory Schemes, III," *Journal of Computational Physics*, Vol. 71, 1987, pp. 231–303.

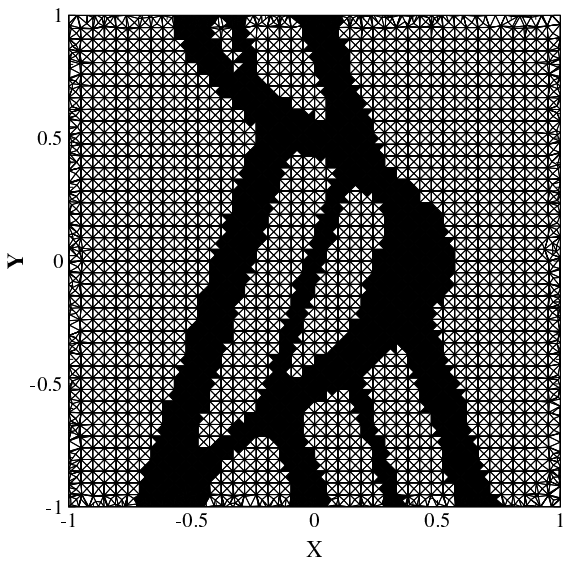

(a) Smoothness indicator. Computational cells highlighted in black were deemed non-smooth by the smoothness indicator.

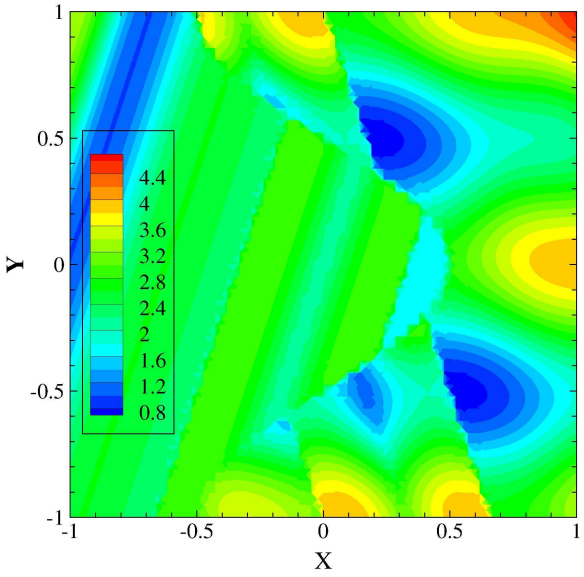

(b) Numerical solution.

Figure 12. Results for CENO reconstruction (with k=4) of Abgrall's function in three dimensions obtained using a mesh with 232,335 tetrahedral cells.

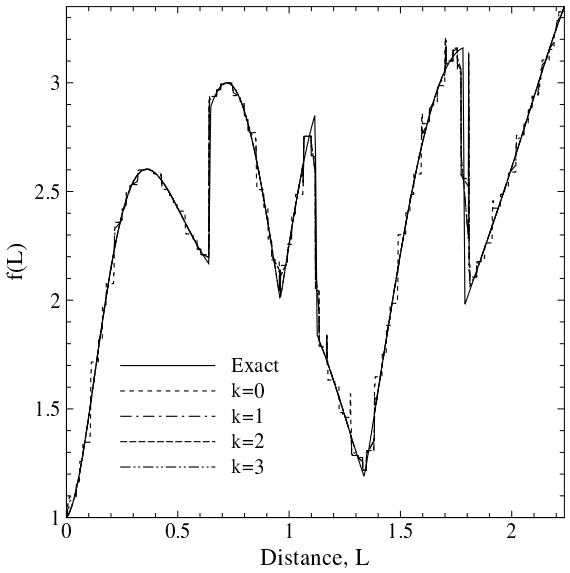

(a) Effect of piecewise polynomial interpolant.

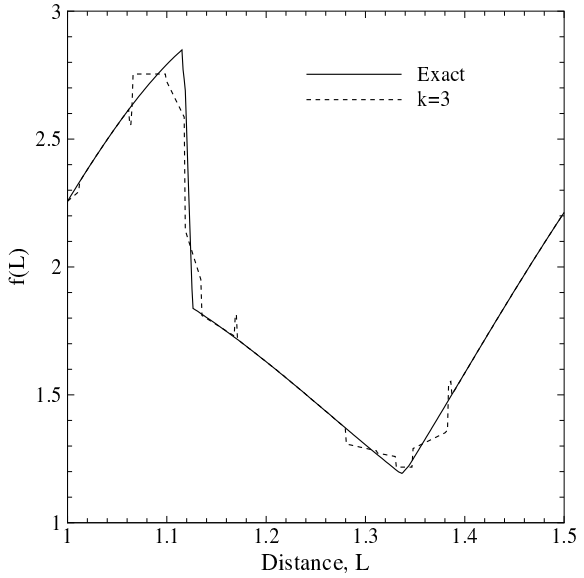

(b) Close up illustrating the limiting procedure.

Figure 13. Reconstructed solution for the Abgrall function in three-dimensions along a line. The solution was obtained using CENO with k=4 on a mesh consisting of 232,335 tetrahedral cells.

[3]Coirier, W. J. and Powell, K. G., "Solution-Adaptive Cartesian Cell Approach for Viscous and Inviscid Flows," *AIAA Journal*, Vol. 34, No. 5, May 1996, pp. 938–945.

[4]Barth, T. J., "Recent Developments in High Order K-Exact Reconstruction on Unstructured Meshes," Paper 93-0668, AIAA, January 1993.

[5]Abgrall, R., "On Essentially Non-Oscillatory Schemes on Unstructured Meshes: Analysis and Implementation," *Journal of Computational Physics*, Vol. 114, 1994, pp. 45–58.

[6]Sonar, T., "On the construction of essentially non-oscillatory finite volume approximations to hyperbolic conservation

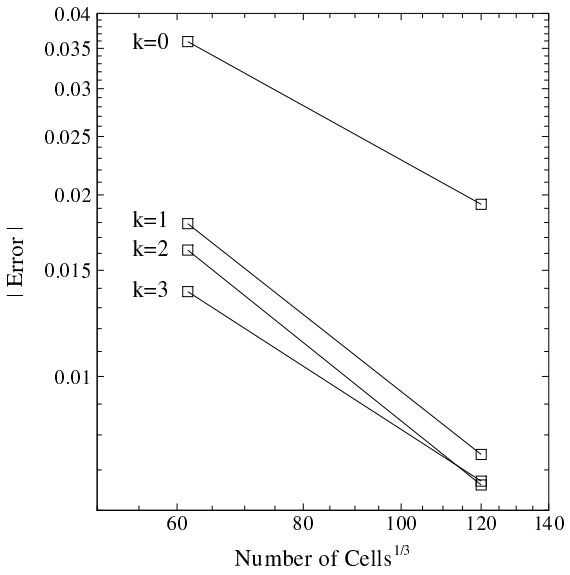

Figure 14. Effect of grid resolution on solution accuracy for CENO reconstruction of the Abgrall function in three-dimensions. Accuracy is measured using the L_1 norm of the error.

laws on general triangulations: polynomial recovery, accuracy and stencil selection," *Computer Methods in Applied Mechanics and Engineering*, 1997, pp. 140–157.

[7]Ollivier-Gooch, C. F., "Quasi-ENO Schemes for Unstructured Meshes Based on Unlimited Data-Dependent Least-Squares Reconstruction," *Journal of Computational Physics*, Vol. 133, 1997, pp. 6–17.

[8]Jiang, G.-S. and Shu, C.-W., "Efficient Implementation of Weighted ENO Schemes," *Journal of Computational Physics*, Vol. 126, 1996, pp. 202–228.

[9]Stanescu, D. and Habashi, W., "Essentially Nonoscillatory Euler solutions on unstructured meshes using extrapolation," *AIAA Journal*, Vol. 36, 1998, pp. 1413–1416.

[10]Friedrich, O., "Weighted Essentially Non-Oscillatory Schemes for the Interpolation of Mean Values on Unstructured Grids," *Journal of Computational Physics*, Vol. 144, 1998, pp. 194–212.

[11]Hu, C. and Shu, C.-W., "Weighted Essentially Non-Oscillatory Schemes on Triangular Meshes," *Journal of Computational Physics*, Vol. 150, 1999, pp. 97–127.

[12]Ollivier-Gooch, C. F. and Van Altena, M., "A High-order Accurate Unstructured Mesh Finite-Volume Scheme for the Advection-Diffusion Equation," *Journal of Computational Physics*, Vol. 181, No. 2, 2002, pp. 729–752.

[13]Cockburn, B. and Shu, C.-W., "TVB Runge-Kutta Local Projection Discontinous Galerkin Finite-Element Method for Conservation Laws II: General Framework," *Mathematics of Computation*, Vol. 52, 1989, pp. 411.

[14]Cockburn, B., Hou, S., and Shu, C.-W., "TVB Runge-Kutta Local Projection Discontinous Galerkin Finite-Element Method for Conservation Laws IV: The Multidimensional Case," *Journal of Computational Physics*, Vol. 54, 1990, pp. 545.

[15]Hartmann, R. and Houston, P., "Adaptive Discontinuous Galerkin Finite Element Methods for the Compressible Euler Equations," *Journal of Computational Physics*, Vol. 183, 2002, pp. 508–532.

[16]Luo, H., Baum, J. D., and Löhner, R., "A Hermite WENO-Based Limiter for Discontinuous Galerkin Method on Unstructured Grids," *Journal of Computational Physics*, Vol. 225, 2007, pp. 686–713.

[17]Gassner, G., Lörcher, F., and Munz, C.-D., "A Contribution to the Construction of Diffusion Fluxes for Finite Volume and Discontinuous Galerkin Schemes," *Journal of Computational Physics*, Vol. 224, 2007, pp. 1049–1063.

[18]Wang, Z. J., "Spectral (Finite) Volume Method for Conservation Laws on Unstructured Grids – Basic Formulation," *Journal of Computational Physics*, Vol. 178, 2002, pp. 210–251.

[19]Wang, Z. J. and Liu, Y., "Spectral (Finite) Volume Method for Conservation Laws on Unstructured Grids – II. Extenstion to Two-Dimensional Scalar Equation," *Journal of Computational Physics*, Vol. 179, 2002, pp. 665–697.

[20]Wang, Z. J., Zhang, L., and Liu, Y., "High-Order Spectral Volume Method for 2D Euler Equations," Paper 2003–3534, AIAA, June 2003.

[21]Wang, Z. J. and Liu, Y., "Spectral (Finite) Volume Method for Conservation Laws on Unstructured Grids – III. One Dimensional Systems and Partition Optimization," *Journal of Scientific Computing*, Vol. 20, No. 1, 2004, pp. 137–157.

[22]Sun, Y., Wang, Z. J., and Liu, Y., "Spectral (finite) volume method for conservation laws on unstructured grids VI: extension to viscous flow," *J. Comput. Phys.*, Vol. 215, No. 1, 2006, pp. 41–58.

[23]Haselbacher, A., "A WENO Reconstruction Algorithm for Unstructed Grids Based on Explicit Stencil Construction," Paper 2005-0879, AIAA, January 2005.

[24]Ivan, L. and Groth, C. P. T., "High-Order Central CENO Finite-Volume Scheme with Adaptive Mesh Refinement," Paper 07–4323, AIAA, June 2007.

[25]Ivan, L., *Development of High-Order CENO Finite-Volume Schemes with Block-Based Adaptive Mesh Refinement*, Ph.D. thesis, University of Toronto, October 2010.

[26]Roe, P. L., "Approximate Riemann Solvers, Parameter Vectors, and Difference Schemes," *Journal of Computational Physics*, Vol. 43, 1981, pp. 357–372.

[27]Roe, P. L. and Pike, J., "Efficient Construction and Utilisation of Approximate Riemann Solutions," *Computing Methods in Applied Science and Engineering*, edited by R. Glowinski and J. L. Lions, Vol. VI, North-Holland, Amsterdam, 1984, pp. 499–518.

[28]Harten, A., Lax, P. D., and van Leer, B., "On Upstream Differencing and Godunov-Type Schemes for Hyperbolic Conservation Laws," *SIAM Review*, Vol. 25, No. 1, 1983, pp. 35–61.

[29]Ivan, L. and Groth, C. P. T., "High-Order Finite-Volume Scheme with Adaptive Mesh Refinement," *Proceedings of the 54th Annual Conference Aerodynamics Symposium of the Canadian Aeronautics and Space Institute, Toronto, Canada, April 24–26, 2007*, CASI, 2007.

[30]Ivan, L. and Groth, C. P. T., "High-Order Central ENO Finite-Volume Scheme with Adaptive Mesh Refinement for the Advection-Diffusion Equation," submitted for presentation at the Fifth International Conference on Computational Fluid Dynamics, Seoul, Korea, July 7–11, 2008, July 2008.

[31]Ivan, L. and Groth, C. P. T., "High-Order Central ENO Finite-Volume Scheme with Adaptive Mesh Refinement for the Advection-Diffusion Equation," Paper, 2008.

[32]Lawson, C. and Hanson, R., *Solving least squares problems*, Prentice-Hall, INC, 1974.

[33]Mavriplis, D. J., "Revisiting the least-squares procedure for gradient reconstruction on unstructured meshes," *AIAA 2003-3986*, 2003.

[34]Venkatakrishnan, V., "On the Accuracy of Limiters and Convergence to Steady State Solutions," Paper 93-0880, AIAA, January 1993.

[35]Geuzaine, C. and Remacle, J.-F., "Gmsh: a three-dimensional finite element mesh generator with built-in pre- and post-processign facilities." *International Journal for Numerical Methods in Engineering*, Vol. 79, No. 11, 2009.

[36]Karypsis, G. and Kumar, V., "Metis - A Software Package for Partitionin Unstructured Graphs, Partitioning Meshes, and Computing Fill-Reducing Orderings of Sparse Matrices." *University of Minnesota, Department of Computer Science / Army HPC Research Center*, 1998.

[37]Sachdev, J. S., Groth, C. P. T., and Gottlieb, J. J., "A Parallel Solution-Adaptive Scheme for Predicting Multi-Phase Core Flows in Solid Propellant Rocket Motors," *International Journal of Computational Fluid Dynamics*, Vol. 19, No. 2, 2005.

[38]Sachdev, J. S. and Groth, C. P. T., "A mesh adjustment scheme for embedded boundaries," *Communications in Computational Physics*, Vol. 2, No. 6, 2007, pp. 1095–1124.

[39]Gao, X. and Groth, C. P. T., "Parallel adaptive mesh refinement scheme for three-dimensional turbulent non-premixed combustion," *46th AIAA Aerospace Sciences Meeting and Exhibit*, Reno, Nevada, 7–10 January 2008, AIAA paper 2008-1017.

[40]Weatherill, N. P., "Lecture Series," VKI.

[41]Barth, T. J., "Aspects of Unstructured Grids and Finite-Volume Solvers for the Euler and Navier-Stokes Equations." *Lecture Notes Presented at the VKI Lecture Series.*, 1995.

[42]Gao, X. and Groth, C. P. T., "A parallel adaptive mesh refinement algorithm for predicting turbulent non-premixed combusting flows," *International Journal of Computational Fluid Dynamics*, Vol. 20, No. 5, 2006, pp. 349–357.

[43]Gao, X. and Groth, C. P. T., "A parallel solution-adaptive method for three-dimensional turbulent non-premixed combusting flows," *Journal of Computational Physics*, Vol. 229, No. 9, 2010, pp. 3250–3275.

[44]Gao, X., Northrup, S., and Groth, C. P. T., "Parallel solution-adaptive method for two-dimensional non-premixed combusting flows," *Progress in Computational Fluid Dynamics*, Vol. 11, No. 2, 2011, pp. 76–95.